

Ultrasmooth Gold Surfaces Prepared by Chemical Mechanical Polishing for Applications in Nanoscience

Michael S. Miller,[†] Michael-Anthony Ferrato,[†] Adrian Niec,[†] Mark C. Biesinger,[‡] and Tricia Breen Carmichael^{*,†}

[†]Department of Chemistry and Biochemistry, University of Windsor, Windsor, Ontario, Canada N9B 3P4

[‡]Surface Science Western, The University of Western Ontario, 999 Collip Circle, LL31 (Lower), London, Ontario, Canada N6G 0J3

S Supporting Information

ABSTRACT: For over 20 years, template stripping has been the best method for preparing ultrasmooth metal surfaces for studies of nanostructures. However, the organic adhesives used in the template stripping method are incompatible with many solvents, limiting the conditions that may subsequently be used to prepare samples; in addition, the film areas that can be reliably prepared are typically limited to $\sim 1 \text{ cm}^2$. In this article, we present chemical–mechanical polishing (CMP) as an adhesive-free, scalable method of preparing ultrasmooth gold surfaces. In this process, a gold film is first deposited by e-beam evaporation onto a 76-mm-diameter silicon wafer. The CMP process removes $\sim 4 \text{ nm}$ of gold from the tops of the grains comprising the gold film to produce an ultrasmooth gold surface supported on the silicon wafer. We measured root-mean-square (RMS) roughness values using atomic force microscopy of 12 randomly sampled $1 \mu\text{m} \times 1 \mu\text{m}$ areas on the surface of the wafer and repeated the process on 5 different CMP wafers. The average RMS roughness was $3.8 \pm 0.5 \text{ \AA}$, which is comparable to measured values for template-stripped gold ($3.7 \pm 0.5 \text{ \AA}$). We also compared the use of CMP and template-stripped gold as bottom electrical contacts in molecular electronic junctions formed from *n*-alkanethiolate self-assembled monolayers as a sensitive test bed to detect differences in the topography of the gold surfaces. We demonstrate that these substrates produce statistically indistinguishable values for the tunneling decay coefficient β , which is highly sensitive to the gold surface topography.



INTRODUCTION

Metallic surfaces with nearly atomic smoothness are essential to the development of a number of nanotechnologies. Fabricating nanostructures on surfaces, imaging nanostructures with scanning probe microscopies, and characterizing nanostructures to develop structure–function relationships all require substrates with a surface roughness that is smaller than the dimensions of the nanostructures being investigated.¹ For over 20 years, the best preparation method has been template stripping, in which a rigid backing layer glued onto a metal film on an ultrasmooth template substrate is stripped away to reveal the ultrasmooth underside of the metal film.^{1–5} Two critical limitations of template stripping, however, impede the continued advancement of nanotechnology: Organic adhesives such as epoxies and polyurethanes used as glues swell in many organic solvents, severely constraining the conditions for subsequent sample preparation. These adhesives can also trap air bubbles and solvent pockets, resulting in subsequent outgassing that is problematic for ultrahigh vacuum systems.⁶ Furthermore, the area of ultrasmooth films that can be prepared is limited to a few centimeters squared.^{2,6,7} Here, we present chemical–mechanical polishing (CMP) as an adhesive-free, scalable method for preparing ultrasmooth gold surfaces. We demonstrate a CMP process that rapidly (<5 min) produces

ultrasmooth gold films with an area of $4.5 \times 10^3 \text{ mm}^2$ and average root-mean-square roughness values of $3.8 \pm 0.5 \text{ \AA}$. A comparison of CMP and template-stripped (TS) gold as bottom electrical contacts in molecular electronic junctions of *n*-alkanethiolate self-assembled monolayers reveals that these substrates produce statistically indistinguishable values for tunneling decay coefficient β , which is highly sensitive to the gold surface topography.⁸

Ultrasmooth metallic substrates are particularly important for studies of charge transport through assemblies of molecules on metallic substrates.^{9,10} In a typical molecular electronic (ME) junction, a self-assembled monolayer (SAM) is chemisorbed to a coinage metal substrate that serves as the bottom electrode, and a top electrode may be chosen from a variety of options, such as a mercury drop, a gallium–indium eutectic (EGaIn) tip, a conducting polymer, a scanning tunneling microscope tip, or a conductive atomic force microscope tip.^{9–11} The topography of the bottom contact is a crucial parameter regardless of the choice of top contact. When the bottom contact is a coinage metal film deposited using e-beam deposition, the surface

Received: August 11, 2014

Revised: October 2, 2014

Published: November 5, 2014

comprises small grains separated by deep grain boundaries. For example, as-deposited (As-Dep) gold films typically comprise grains that are ~ 50 nm in diameter separated by grain boundaries that are ~ 10 nm deep with a root-mean-square (RMS) roughness of ~ 30 – 80 Å.^{4,12–14} *n*-Alkanethiolate SAMs formed on As-Dep surfaces possess regions of disorder because the adsorbates cannot pack at the grain boundaries. This topographically induced disorder results in a variation of the thickness of the SAM across the surface, with thin disordered regions at grain boundaries.^{5,15} According to the simplified version of the Simmons equation (eq 1), which is the most common approach to model charge transport, small changes in SAM thickness (d) due to topographically induced disorder cause an exponential change in the tunneling current density J (A cm^{-2}); J_0 (A cm^{-2}) is the limiting value of current for a hypothetical junction with no hydrocarbon present ($d = 0$), and β (nC^{-1} or Å^{-1}) is the tunneling decay constant:^{16,17}

$$J = J_0 e^{-\beta d} \quad (1)$$

Thus, the variation in SAM thickness results in a substantial variation in the measured current densities, which makes the interpretation of ME junction data challenging. A key innovation in the development of ME junctions was the replacement of As-Dep metal electrodes with ultrasmooth metal electrodes prepared by template stripping.^{5,8,10,18,19} The TS metal surface is smoother than As-Dep surfaces, with larger grains separated by shallower grain boundaries. For example, typical TS gold surfaces consist of large (50–500 nm diameter), atomically flat terraces that vary by only a few atomic steps in height, resulting in an RMS roughness of 2–10 Å.^{2–4,13,14,20} SAMs formed on TS metal surfaces possess fewer topographically induced defects, which consequently increases the yield of viable junctions (i.e., those without electrical shorts) and reduces the variation in measured current densities compared to ME junctions formed using As-Dep substrates.^{5,18} This improvement has been demonstrated with different top contact types (e.g., hard scanning probe tips and soft liquid metal drops), junction areas (several nanometers to several micrometers), and bottom electrode materials (Ag and Au).^{5,8,10,18,19}

The introduction of TS substrates in ME junctions has enabled a meaningful statistical analysis of junction data, particularly when used in combination with a “soft” top contact made from EGaIn.²¹ A key property of EGaIn is the formation of a Ga_2O_3 layer (~ 0.7 nm thick) on the surface that enables the fabrication of small (~ 25 nm diameter) tips.²² Furthermore, the resistance of the Ga_2O_3 layer does not contribute to the resistance of the junction.^{23,24} The EGaIn/ Ga_2O_3 contact makes it practical to collect large numbers of $J(V)$ data; the combination of a TS metal bottom contact and EGaIn/ Ga_2O_3 top contact has thus opened the way to systematic studies of charge transport across organic thin films. A comparison of $J(V)$ data sets from junctions formed using different molecules has statistically distinguished effects such as rectification,^{25–30} the odd–even effect,^{30,31} different torsional angles of biphenyl groups,³² quantum interference,³³ and the effect of the molecular structure of the SAM and its interfaces with the electrodes.^{34–39} We may now be poised to exploit the huge variety of molecular structures that can be chemically synthesized to cultivate a deep understanding of the mechanisms of charge transport and pursue molecular devices that outperform silicon. However, the critical limitation of TS

metal contacts—the adhesive—presents a serious challenge when forming SAMs of complex molecules, such as large conjugated systems incorporating electroactive functionalities such as ferrocenes or porphyrins.^{25,26,28,40–47} Typical organic adhesives, such as polyurethanes and epoxies, used to glue a rigid backing layer to the back side of the ultrasmooth metal film are compatible with ethanolic solutions of *n*-alkanethiols commonly used to prepare SAMs; however, the strong organic or chlorinated solvents that will likely be necessary to form SAMs of complex molecules swell this adhesive and cause topographical changes to the TS gold film over a relatively short time. Figure S1 shows that pinhole or blister defects arise when TS gold is immersed in toluene for 24 h. The damage caused by immersion in halogenated solvents is more severe: dissolution of the adhesive destroys the sample after only 3 h in chloroform or 1 h in dichloromethane. The incompatibility of the adhesive with these solvents will only be exacerbated with complex molecules of very low solubility, which may require heating to keep them in solution.^{6,40,41,48} There have been efforts to replace organic adhesives with innocuous alternatives increase the fabrication time by adding processing steps, (e.g., additional metal deposition steps by evaporation¹² or electroplating⁴⁸). Efforts to avoid adhesive altogether through a cold-welding process require additional metal evaporation steps⁴⁹ or specialized handling to avoid problematic surface contamination.⁶ Other alternatives to organic adhesives such as solder¹⁴ or liquid glass⁵⁰ can be applied relatively simply; nonetheless, these methods have been demonstrated only on small (~ 1 cm^2) areas.

Here, we report a simple, scalable, and adhesive-free alternative to template stripping based on CMP to produce ultrasmooth gold surfaces. CMP is an essential process in microelectronics manufacturing, where it is used to remove overburden metal or oxide in damascene/dual damascene processes rapidly and to planarize interlevel dielectrics for shallow trench isolation.⁵¹ CMP removes material through a combination of chemical etching and abrasive polishing with a planar polishing pad. During the CMP process, the polishing pad contacts asperities on the wafer and preferentially removes material from these areas, thus planarizing the surface both locally and globally. Despite these favorable attributes and heavy use by the microelectronics industry, the use of CMP to prepare ultrasmooth metallic surfaces for studies of nanostructures has been overlooked except for a 2005 report by Islam et al., which reports a CMP process to reduce the grain height of as-deposited platinum surfaces.⁵² We present a CMP process to prepare ultrasmooth gold by polishing the surface of As-Dep gold. Gold has long been the substrate of choice for studies of SAMs because it is chemically inert, allowing it to be handled under ambient conditions, and because of its high affinity for thiols.¹⁵ We use atomic force microscopy to show that CMP gold, like TS gold, presents an ultrasmooth surface. SAMs of *n*-alkanethiols formed on CMP and TS gold are indistinguishable according to reflection–absorption infrared spectroscopy (RAIRS); furthermore, the properties of ME junctions formed from SAMs on CMP and TS gold with EGaIn top contacts are also statistically indistinguishable. In particular, values of the tunneling decay coefficient β , which is highly sensitive to the gold surface topography,⁸ indicate that CMP gold is an effective ultrasmooth substrate for ME junctions, unhindered by the solvent restrictions associated with TS gold.

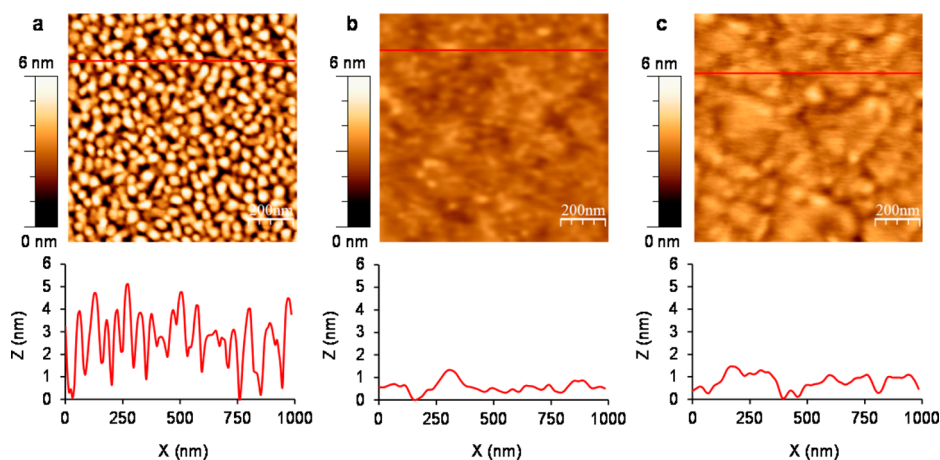


Figure 1. Surface topography of As-Dep, CMP, and TS gold. AFM topographic images (top) and corresponding line-scan profiles (bottom) of (a) As-Dep gold, (b) CMP gold, and (c) TS gold.

EXPERIMENTAL SECTION

All chemicals were purchased commercially and used as received unless otherwise specified. All *n*-alkanethiols were purified by silica gel column chromatography using gravity elution with 100% hexanes. Additional experimental details, instrumental protocols, purification methods for *n*-alkanethiols, and NMR spectroscopic data are provided in the Supporting Information.

Preparation of CMP Slurry. Hydrophilic fumed silica (5 g, Aerosil 200), I₂ (0.03 g), KI (0.3 g), citric acid (4.1 g), and trisodium citrate (0.925 g) were added to 500 mL of deionized water. The mixture was simultaneously sonicated and bubbled with dry nitrogen for 1 h.

Preparation of As-Dep and CMP Gold. As-Dep gold substrates were prepared by depositing 2 nm of titanium followed by 50 nm of gold onto 75 -mm-diameter silicon wafers using an e-beam evaporator. Prior to CMP, As-Dep gold substrates were bonded to a 75 -mm-diameter glass carrier disc (Logitech Ltd.) using low-melting-point quartz wax (South Bay Technologies Inc.) at 100 °C on a hot plate. After cooling, it was held in vacuum contact with the chuckface of a PP5 polishing jig (Logitech Ltd., U.K.) and placed face down onto a 12-in.-diameter polyurethane polishing cloth (Chemcloth, Logitech Ltd.) adhered to the stainless steel platen of a PM5 lapping and polishing system (Logitech Ltd) with <1 psi downforce. Polishing slurry was dripped from a PM5 Syton feed unit at a rate of 2 to 3 drops/s onto a polishing cloth, and the As-Dep gold substrate was polished for 4 min with a platen rotational speed of 25 rpm and a jig head-sweep speed of 5 mm/s. CMP gold substrates were removed from the glass carrier disc by heating to 100 °C on a hot plate for 5 min to melt the bonding wax. Residual wax was removed with toluene. The CMP gold substrates were then sonicated for 15 min in a detergent solution (5 g of Sparkleen from Fisher Scientific dissolved in 200 mL of deionized water) at 75 °C, and then rinsed with deionized water and methanol and dried under a stream of dry nitrogen.

Preparation of TS Gold Substrates. TS gold substrates were fabricated according to published procedures.¹⁴ Gold (500 nm) was deposited onto a 75-mm-diameter silicon wafer using an e-beam evaporator, and then a drop (5 μ L) of UV-curable adhesive (NOA 83H, Norland Optical) was applied to the gold surface, followed by a 1 cm \times 1 cm glass substrate. After the adhesive was cured using a 100 W UV lamp for 15 min, the glass substrate was stripped from the silicon wafer using a scalpel.

Formation of C_nSH SAMs. CMP gold substrates were sonicated in anhydrous ethanol for 5 min and then placed in a 1 mM solution of the appropriate *n*-alkanethiol in ethanol for 12 h under nitrogen. TS gold substrates were stripped from a silicon wafer and immediately placed into a 3 mM solution of the appropriate *n*-alkanethiol in ethanol for 3 h under nitrogen.

Electrical Measurements. A conical EGaIn/Ga₂O₃ top electrode was fabricated by extruding a drop (\sim 0.5 μ L) of EGaIn from a 10 μ L

gastight syringe, bringing it into contact with a sacrificial gold substrate, and slowly withdrawing the syringe from the substrate. ME junctions were formed according to the procedure described by Thuo et al.³¹ by gently bringing the EGaIn/Ga₂O₃ tip into contact with the SAM. Contact between the tip and the SAM was judged by the convergence of the tip with its reflected image on the substrate surface to give electrical contact, which was confirmed by passing a current through the junction. Once the junction was formed, a Keithley 6430 source meter applied a bias sweep from 0 \rightarrow -0.5 \rightarrow +0.5 \rightarrow 0 V across the junction and measured the current. Current densities were calculated by assuming a circular contact area; the diameter was measured using an Allied Vision Technologies Stingray F-046 high-magnification CCD camera. After the EGaIn/Ga₂O₃ top electrode was placed in contact with the SAM, the presence of a molecular tunnel junction was confirmed by measuring a single *J*(*V*) trace. A working junction was defined as a sigmoidally shaped *J*(*V*) trace, and a short circuit was defined as a straight line in which the current reached the compliance of the source meter (105 mA). After establishing a working tunnel junction, 20 subsequent *J*(*V*) traces were measured from the same area. A minimum of 13 randomly sampled tunnel junctions totalling a minimum of 260 *J*(*V*) traces were measured for each C_nSH SAM on CMP and TS gold. We measured a maximum of five junctions before fabricating a new EGaIn/Ga₂O₃ tip. The nonshorting junction yield is defined as the number of junctions that short circuit divided by the total number of junctions sampled, after the first working junction (21 *J*(*V*) traces) of that particular sample has been established. Charge transport data for SAMs on CMP and TS gold are summarized in Tables S3 and S4.

RESULTS AND DISCUSSION

CMP Process for Ultrasmooth Gold Surfaces. We developed a CMP process to planarize the surface of an As-Dep gold film prepared by e-beam evaporation of 2 nm of titanium followed by 50 nm of gold onto a 76-mm-diameter silicon wafer. This As-Dep surface consists of gold grains with diameters of \sim 50 nm, separated by grain boundaries that are \sim 5 to 6 nm deep (Figure 1a). Accordingly, we designed a CMP process to produce a flat, ultrasmooth surface by polishing the gold down from the tops of the grains to approximately the bottom of the grain boundaries, corresponding to the removal of \sim 5 nm in film thickness. In CMP, the sample to be polished is mounted onto a polishing jig and placed in contact with a polyurethane polishing pad. An aqueous slurry is continuously dripped onto the polishing pad while the polishing pad and the jig are rotated and the jig is swept linearly across the pad. Slurries for the CMP of metal films use a chemical etchant to

oxidize the metal surface. The resulting metal ions are then removed by synergistic chemical dissolution (often assisted by complexing ligands in the slurry) and mechanical abrasion by the polishing pad and abrasive particles, such as alumina or silica, in the slurry.⁵³ To remove only ~ 5 nm of material, we designed a CMP process with a low removal rate by employing a slurry with a low etchant concentration in combination with a low downforce (<1 psi) between the surface and polishing pad. We used dilute iodine triiodide, a standard gold etchant, to oxidize gold atoms on the surface to produce gold(I) iodide.⁵⁴ Citric acid/trisodium citrate buffer (50 mM, pH 3) provided a stable pH throughout the CMP process to keep the oxidation potential of gold consistent.⁵¹ Citric acid also complexes the gold ions generated on the surface of the film to improve solubility and prevent redeposition.⁵¹ Finally, we used hydrophilic fumed silica with a mean primary particle size of 12 nm as the abrasive and sonicated the slurry prior to polishing to reduce particle aggregation. The sonication step reduces the average aggregate size to ~ 25 nm, which prevents scratching of the gold surface during polishing.⁵⁵ After CMP, we used a cleaning process designed to remove residual slurry and dissolve residual KI and I_2 on the CMP gold surface in water and methanol.

Topography of CMP Gold. A comparison of tapping mode atomic force microscopy (AFM) images of As-Dep and CMP gold surfaces shows that removing the tops of the gold grains by CMP produces a flat, smooth surface (Figure 1a,b). The distinct gold domains of As-Dep gold, which are due to the island growths of gold during e-beam evaporation, become far less pronounced after the CMP process. CMP reduces the RMS roughness of the gold surface over a $1 \mu\text{m}^2$ area from 11.5 ± 1.6 Å for As-Dep gold to 3.8 ± 0.5 Å for CMP gold. Line scans taken from the AFM images more clearly depict how CMP changes the topography of As-Dep gold and provide data to estimate the thickness of gold removed by CMP. We measured maximum peak-to-valley distances of each of 45 line scans that were obtained from AFM images taken from 3 different regions on 3 different samples each of As-Dep and CMP gold. The average maximum peak-to-valley distances were 5.5 ± 0.6 nm for As-Dep gold and 2.1 ± 0.6 nm for CMP gold, corresponding to a removal of roughly 4 nm of gold by CMP.

A comparison of AFM images of CMP and TS gold (Figure 1b,c) shows that although both surfaces can be described as ultrasmooth according to roughness measurements, they differ in the distribution of grain sizes that comprise them. CMP and TS gold have comparable RMS surface roughness values of 3.8 ± 0.5 and 3.7 ± 0.5 Å, respectively, measured over a $1 \mu\text{m} \times 1 \mu\text{m}$ area and identical average maximum peak-to-valley distances measured from AFM cross sections (2.1 ± 0.6 and 2.1 ± 0.5 nm, respectively). Two-sample *t* tests for both the RMS roughness values and maximum peak-to-valley distances confirmed that there was no statistically significant difference between the data sets on CMP and TS gold ($p > 0.5$). The root mean square is a statistical measure of roughness commonly used to compare surfaces, but RMS roughness values can be misleading because they do not describe the horizontal spatial distribution of surface features. For example, surfaces with a wide, hilly topography can have an RMS roughness value identical to a surface with narrower and sharper peaks as long as the hills or peaks deviate from the mean plane by the same amount on average. We therefore analyzed the diameters of the grains comprising CMP and TS gold to reveal differences between these surfaces. The diameters of 60 grains measured

from AFM line scans taken from CMP and TS gold samples show a similar range of grain diameters: CMP grain diameters range from 19–250 nm, and TS grain diameters range from 19–267 nm. On both surfaces, roughly 50% of the grains measured have diameters of between 50 and 99 nm. However, CMP and TS gold differ in their proportions of small (diameters <50 nm) and large (>100 nm) grains that comprise these surfaces: 38% of CMP gold grains have diameters of <50 nm, compared to 12% of TS gold grains in this size range. Conversely, 42% of TS gold grains have diameters of >100 nm, compared to only 12% of CMP gold grains in this size range.

Reliability of the CMP Process. The CMP process produces ultrasmooth gold surfaces over the area of a 76-mm-diameter Si wafer. We assessed the precision of the CMP process over this $4.5 \times 10^3 \text{ mm}^2$ area and wafer to wafer by measuring the RMS roughness of 12 randomly sampled $1 \mu\text{m} \times 1 \mu\text{m}$ areas from 4 different geometric locations that spanned the surface of the wafer ($\sim 15, 30, 45,$ and 60 mm from the wafer flat) and repeated the process on 5 different CMP wafers to generate a total of 60 roughness measurements. The results of this study are summarized in Table 1. A histogram

Table 1. Summary of Root-Mean-Square Roughness Measurements of CMP Au

wafer number	μR_{RMS} (Å)	σR_{RMS} (Å)	coefficient of variation (%)
1	4.1	0.3	7
2	4.0	0.6	15
3	3.8	0.3	8
4	3.5	0.4	11
5	3.6	0.2	6
all 60 scans	3.8	0.5	13

representing the 60 RMS roughness values (Figure 2) shows a normal distribution with all roughness values falling within a range that can be considered to be ultrasmooth (2.8 to 5.2 Å). The average (μ) of these roughness measurements is 3.8 ± 0.5 Å, corresponding to a coefficient of variation of 13%. We also determined the precision of the polishing process across a wafer by calculating the coefficient of variation of the roughness

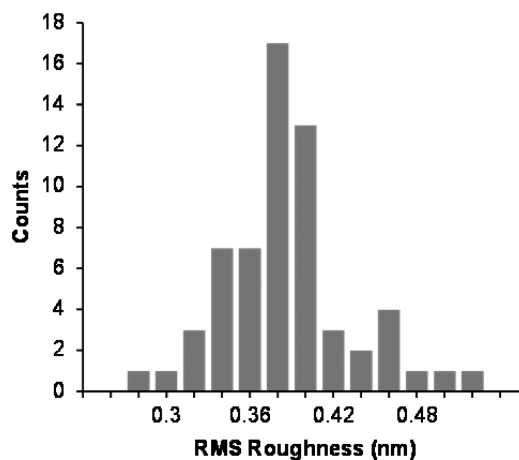


Figure 2. Reliability of the CMP process for preparing ultrasmooth gold. Histogram of RMS surface roughness values measured from 12 randomly sampled $1 \mu\text{m} \times 1 \mu\text{m}$ areas on a CMP gold wafer and repeated on 5 different CMP wafers to generate a total of 60 roughness measurements. The y axis of the histogram corresponds to the number of counts for a given statistical bin.

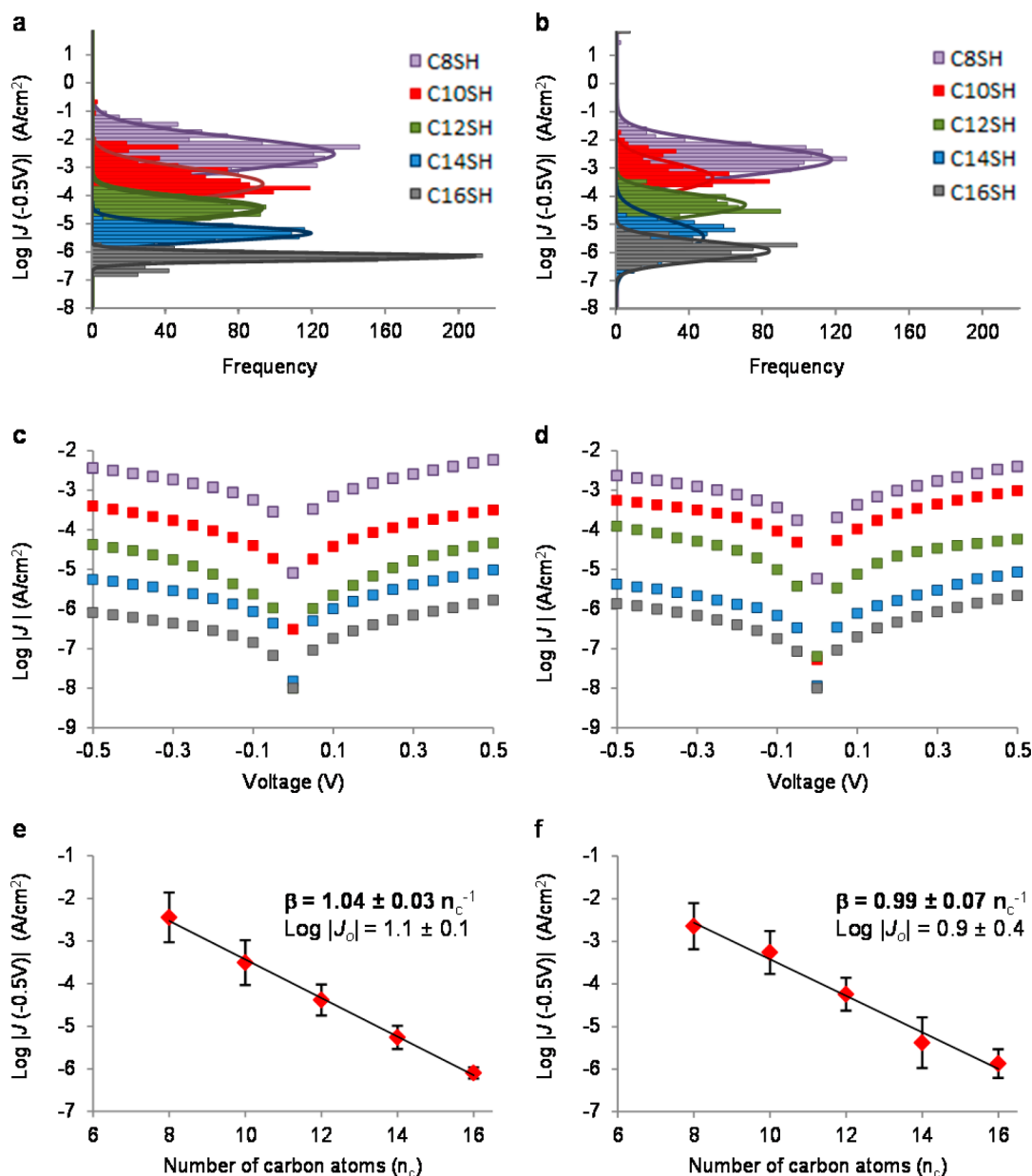


Figure 3. Charge-transport data for ME junctions of C_n SH SAMs ($n = 8, 10, 12, 14, 16$) on CMP and TS gold. (a, b) Histograms of $\log |J| (-0.5 V)$ fitted with unimodal Gaussian curves. The x axes correspond to the number of counts for a given statistical bin. (c, d) Plots of the \log (average $J(V)$) curves. (e, f) Plots of the Gaussian mean values of $\log |J|$ at $-0.5 V$ vs the number of carbon atoms in the C_n SH SAM. a, c, and e are for CMP gold; b, d, and f are for TS gold.

measurements collected for each CMP wafer. These values ranged from 6 to 15%, indicating that the CMP process generates uniform, ultrasmooth surfaces that are usable over the entire $4.5 \times 10^3 \text{ mm}^2$ surface of the wafer.

Chemical Composition of the Surface of CMP Gold.

We used X-ray photoelectron spectroscopy (XPS) to characterize the chemical state of the gold surface after the CMP process. The XPS survey scan of CMP gold (Figure S2a) shows signals due to gold, carbon, oxygen, and sulfur, consistent with the adsorption of adventitious organic materials on the gold surface. The survey scan also shows 0.4 atom % iodine. An XPS thickogram calculation (Figure S2b, Table S1) estimates the thickness of the iodine layer to be $<0.1 \text{ \AA}$, indicating submonolayer surface coverage.^{56,57} It is not possible to determine the binding state of the iodine species because of

the negligible differences in binding energies of physisorbed and chemisorbed iodine on gold.⁵⁸ Because n -alkanethiolates efficiently displace physisorbed contaminants on the gold surface as a result of the high affinity of sulfur for gold,¹⁵ we formed an n -hexadecanethiolate SAM on the CMP gold surface to distinguish between physisorbed and chemisorbed iodine species. The XPS survey scan (Figure S3a) shows the elements consistent with SAM formation along with 0.4 atom % iodine. The thickness of this iodine layer estimated by the thickogram method is $<0.1 \text{ \AA}$ (Figure S3b, Table S1), unchanged from the post-CMP gold surface. The persistence of the iodine species after SAM formation is consistent with a chemisorbed iodine species on the surface of CMP gold, which we believe is likely residual AuI on the gold surface. This species, however, does not prevent SAM formation nor does it compromise the

organization of *n*-alkanethiolate adsorbates on the surface: We formed the series of C_n SH SAMs ($n = 8, 10, 12, 14, 16$; the number of carbon atoms in the alkyl chain) on CMP and TS gold and compared the frequencies of the asymmetric and symmetric methylene C–H stretching modes in RAIR spectra, which are diagnostic of alkyl chain crystallinity.⁵⁹ The data (Table S2) show that the C–H stretching frequencies of SAMs on CMP and TS gold are indistinguishable, which implies that CMP and TS surfaces support the formation of SAMs with similar adsorbate packing densities and conformational organization.

CMP Gold as Bottom Contacts in ME Junctions. ME junctions of C_n SH SAMs sandwiched between two metallic electrodes are an effective test bed to compare the effect of differences in topography of CMP and TS gold. Possible metrics for comparison include the values determined for J_0 and β and nonshorting ME junction yield. Values of J_0 are highly dependent on the contact area of the top electrode²³ and thus less useful for distinguishing between topographical differences of the bottom contact. Recently, however, Yuan et al. showed that the topography of the underlying silver or gold substrate—the surface roughness, grain size, and the width of the grain boundaries—has a profound effect on the tunneling decay coefficient β and a measurable effect on the yield of ME junctions derived from C_n SH SAMs: rough surfaces with many grain boundaries produce low β values (0.4 – 0.5 nC^{-1}); smooth surfaces with fewer grain boundaries produce β values of ~ 1.0 nC^{-1} .⁸ Similarly, junction yields increased from 60% for rough, As-Dep silver surfaces to nearly 100% for TS silver.¹⁹ We determined junction yields and β values for C_n SH SAMs ($n = 8, 10, 12, 14, 16$) on CMP and TS gold with a top contact formed from a conical EGaIn/Ga₂O₃ tip brought into gentle contact with the SAM surface according to previously reported procedures.^{22,31,39} Figure 3a,b shows histograms of all of the currents measured at -0.5 V for SAMs on CMP and TS gold. We fitted unimodal Gaussian curves to these data and used them to obtain the log-mean (μ_{\log}) of the value of J and the log-standard deviation (σ_{\log}) (Table 2).²¹ Repeating this procedure

Table 2. Summary of Charge-Transport Data at $V = -0.5$ V for C_n SH SAMs Formed on CMP and TS Gold Surfaces

<i>n</i>	CMP gold			TS gold		
	μ_{\log}	σ_{\log}	junction yield (%)	μ_{\log}	σ_{\log}	junction yield (%)
8	-2.44	0.58	87	-2.64	0.54	88
10	-3.51	0.53	96	-3.26	0.50	81
12	-4.38	0.37	94	-4.24	0.38	76
14	-5.26	0.27	94	-5.38	0.59	95
16	-6.10	0.13	100	-5.87	0.34	87

for all applied biases between -0.5 and 0.5 V produces the log(average $J(V)$) curves in Figure 3c,d. The junction data at $V = -0.5$ V (Table 2) show that CMP and TS gold produce similar ME junctions at each chain length: Values of μ_{\log} (-0.5 V) of SAMs on CMP gold are within $\pm 1\sigma_{\log}$ of SAMs on TS gold; moreover, the range of σ_{\log} (-0.5 V) on CMP gold (0.13 – 0.58) is similar to that of TS gold (0.34 – 0.59), suggesting that SAMs on CMP and TS gold have similar average tunneling barrier thicknesses and thus similar defect densities in the SAMs. Two-sample *t* tests of μ_{\log} (-0.5 V) revealed no statistically significant difference for chain lengths of 8, 10, 12, and 14 carbons on CMP and TS gold. The

junction data for the C16 chain length on CMP and TS gold at $V = -0.5$ does appear different on a statistically significant level ($p = 0.025$); however, this is most likely due to the unusually small standard deviation for the data collected on CMP gold. CMP and TS gold also give comparable junction yields. Plots of $\log |J|$ versus nC in Figure 3e,f provide β values of 1.04 ± 0.03 C^{-1} for CMP gold and 0.99 ± 0.07 C^{-1} for TS gold. These values fall within with the widely accepted range of β values (0.90 – 1.1 nC^{-1}) measured for different ME junction structures²³ and also agree with β values of *n*-alkanethiolate SAMs on TS gold measured using a flattened EGaIn tip.⁶⁰ More importantly, agreement between the β values of CMP and TS gold indicate that these substrates have comparable topographies and that CMP gold is an effective, adhesive-free substitute for TS gold in ME junction studies.

CONCLUSIONS

Although template stripping has served the needs of fundamental nanoscience research for many years, the ability to fabricate molecular junctions and other nanostructures over large areas without a restriction on the type of processing solvent is a necessity for the continued development of these technologies and their implementation in practical applications. The CMP method reported here is an enabling technology for nanoscience: it provides adhesive-free ultrasmooth surfaces that are not damaged or altered by organic and halogenated solvents (Figure S1). CMP is fully compatible with commercial semiconductor manufacturing and is potentially scalable to state-of-the-art 300-mm-diameter wafers (7.1×10^4 mm²) because of the high-precision CMP tools developed by the semiconductor industry. We expect that the development of CMP methods to prepare ultrasmooth films of metals other than gold will provide ultrasmooth surfaces that are useful in a wide variety of nanoscience studies.

ASSOCIATED CONTENT

Supporting Information

Experimental details, optical micrographs of CMP and TS gold after immersion in solvents, XPS survey scans and graphical representation of thickogram calculations, thickogram parameters, reflection–absorption infrared spectroscopic data, summary of charge-transport measurements, and ¹H NMR spectra. This material is available free of charge via the Internet at <http://pubs.acs.org>.

AUTHOR INFORMATION

Corresponding Author

*E-mail: tbcarmic@uwindsor.ca.

Notes

The authors declare no competing financial interest.

ACKNOWLEDGMENTS

This research was supported by the National Sciences and Engineering Research Council of Canada (NSERC) and by the Ontario Ministry of Research and Innovation through an Early Researcher Award to T.B.C. M.S.M. is grateful for the award of an NSERC postgraduate doctoral scholarship. M.-A.F. is grateful for the award of an Ontario Graduate Scholarship. We thank Dr. Heng-Yong Nie at Surface Science Western for atomic force microscopy.

REFERENCES

- (1) Vogel, N.; Zieleniecki, J.; Koper, I. As Flat as it Gets: Ultrasoft Surfaces from Template-Stripping Procedures. *Nanoscale* **2012**, *4*, 3820–3832.
- (2) Hegner, M.; Wagner, P.; Semenza, G. Ultralarge Atomically Flat Template-Stripped Au Surfaces for Scanning Probe Microscopy. *Surf. Sci.* **1993**, *291*, 39–46.
- (3) Wagner, P.; Zaugg, F.; Kernen, P.; Hegner, M.; Semenza, G. ω -Functionalized Self-Assembled Monolayers Chemisorbed on Ultraflat Au(111) Surfaces for Biological Scanning Probe Microscopy in Aqueous Buffers. *J. Vac. Sci. Technol., B* **1996**, *14*, 1466–1471.
- (4) Naumann, R.; Schiller, S. M.; Giess, F.; Grohe, B.; Hartman, K. B.; Kärcher, I.; Köper, I.; Lübken, J.; Vasilev, K.; Knoll, W. Tethered Lipid Bilayers on Ultraflat Gold Surfaces. *Langmuir* **2003**, *19*, 5435–5443.
- (5) Weiss, E. A.; Chiechi, R. C.; Kaufman, G. K.; Kriebel, J. K.; Li, Z.; Duati, M.; Rampi, M. A.; Whitesides, G. M. Influence of Defects on the Electrical Characteristics of Mercury-Drop Junctions: Self-Assembled Monolayers of *n*-Alkanethiolates on Rough and Smooth Silver. *J. Am. Chem. Soc.* **2007**, *129*, 4336–4349.
- (6) Blackstock, J. J.; Li, Z.; Jung, G.-y. Template stripping using cold welding. *J. Vac. Sci. Technol., A* **2004**, *22*, 602–605.
- (7) Blackstock, J. J.; Li, Z.; Freeman, M. R.; Stewart, D. R. Ultra-Flat Platinum Surfaces from Template-Stripping of Sputter Deposited Films. *Surf. Sci.* **2003**, *546*, 87–96.
- (8) Yuan, L.; Jiang, L.; Zhang, B.; Nijhuis, C. A. Dependency of the Tunneling Decay Coefficient in Molecular Tunneling Junctions on the Topography of the Bottom Electrodes. *Angew. Chem., Int. Ed.* **2014**, *53*, 3377–3381.
- (9) McCreery, R. L.; Yan, H.; Bergren, A. J. A Critical Perspective on Molecular Electronic Junctions: There is Plenty of Room in the Middle. *Phys. Chem. Chem. Phys.* **2013**, *15*, 1065–1081.
- (10) McCreery, R. L.; Bergren, A. J. Progress with Molecular Electronic Junctions: Meeting Experimental Challenges in Design and Fabrication. *Adv. Mater.* **2009**, *21*, 4303–4322.
- (11) McCreery, R. L. Molecular Electronic Junctions. *Chem. Mater.* **2004**, *16*, 4477–4496.
- (12) Wagner, P.; Hegner, M.; Guentherodt, H.-J.; Semenza, G. Formation and in Situ Modification of Monolayers Chemisorbed on Ultraflat Template-Stripped Gold Surfaces. *Langmuir* **1995**, *11*, 3867–3875.
- (13) Miller, M. S.; Juan, R. R. S.; Ferrato, M.-A.; Carmichael, T. B. New Dialkylthiophosphinic Acid Self-Assembled Monolayers (SAMs): Influence of Gold Substrate Morphology on Adsorbate Binding and SAM Structure. *Langmuir* **2011**, *27*, 10019–10026.
- (14) Weiss, E. A.; Kaufman, G. K.; Kriebel, J. K.; Li, Z.; Schalek, R.; Whitesides, G. M. Si/SiO₂-Templated Formation of Ultraflat Metal Surfaces on Glass, Polymer, and Solder Supports: Their Use as Substrates for Self-Assembled Monolayers. *Langmuir* **2007**, *23*, 9686–9694.
- (15) Love, J. C.; Estroff, L. A.; Kriebel, J. K.; Nuzzo, R. G.; Whitesides, G. M. Self-Assembled Monolayers of Thiolates on Metals as a Form of Nanotechnology. *Chem. Rev.* **2005**, *105*, 1103–1170.
- (16) Simmons, J. G. *Conduction in Thin Films*; Mills and Boon Ltd.: London, 1971.
- (17) Lamb, D. R. *Electrical Conduction Measurements in Thin Insulating Films*; Methuen and Co.: London, 1968.
- (18) Engelkes, V. B.; Beebe, J. M.; Frisbie, C. D. Analysis of the Causes of Variance in Resistance Measurements on Metal–Molecule–Metal Junctions Formed by Conducting-Probe Atomic Force Microscopy. *J. Phys. Chem. B* **2005**, *109*, 16801–16810.
- (19) Yuan, L.; Jiang, L.; Thompson, D.; Nijhuis, C. A. On the Remarkable Role of Surface Topography of the Bottom Electrodes in Blocking Leakage Currents in Molecular Diodes. *J. Am. Chem. Soc.* **2014**, *136*, 6554–6557.
- (20) Gupta, P.; Loos, K.; Korniaikov, A.; Spagnoli, C.; Cowman, M.; Ulman, A. Facile Route to Ultraflat SAM-Protected Gold Surfaces by “Amphiphile Splitting”. *Angew. Chem., Int. Ed.* **2004**, *43*, 520–523.
- (21) Reus, W. F.; Nijhuis, C. A.; Barber, J. R.; Thuo, M. M.; Tricard, S.; Whitesides, G. M. Statistical Tools for Analyzing Measurements of Charge Transport. *J. Phys. Chem. C* **2012**, *116*, 6714–6733.
- (22) Chiechi, R. C.; Weiss, E. A.; Dickey, M. D.; Whitesides, G. M. Eutectic Gallium–Indium (EGaIn): A Moldable Liquid Metal for Electrical Characterization of Self-Assembled Monolayers. *Angew. Chem., Int. Ed.* **2008**, *47*, 142–144.
- (23) Simeone, F. C.; Yoon, H. J.; Thuo, M. M.; Barber, J. R.; Smith, B.; Whitesides, G. M. Defining the Value of Injection Current and Effective Electrical Contact Area for EGaIn-Based Molecular Tunneling Junctions. *J. Am. Chem. Soc.* **2013**, *135*, 18131–18144.
- (24) Cademartiri, L.; Thuo, M. M.; Nijhuis, C. A.; Reus, W. F.; Tricard, S.; Barber, J. R.; Sodhi, R. N. S.; Brodersen, P.; Kim, C.; Chiechi, R. C.; Whitesides, G. M. Electrical Resistance of AgTSS-(CH₂)_{n-1}CH₃//Ga₂O₃/EGaIn Tunneling Junctions. *J. Phys. Chem. C* **2012**, *116*, 10848–10860.
- (25) Nijhuis, C. A.; Reus, W. F.; Whitesides, G. M. Mechanism of Rectification in Tunneling Junctions Based on Molecules with Asymmetric Potential Drops. *J. Am. Chem. Soc.* **2010**, *132*, 18386–18401.
- (26) Nijhuis, C. A.; Reus, W. F.; Siegel, A. C.; Whitesides, G. M. A Molecular Half-Wave Rectifier. *J. Am. Chem. Soc.* **2011**, *133*, 15397–15411.
- (27) Nijhuis, C. A.; Reus, W. F.; Barber, J. R.; Dickey, M. D.; Whitesides, G. M. Charge Transport and Rectification in Arrays of SAM-Based Tunneling Junctions. *Nano Lett.* **2010**, *10*, 3611–3619.
- (28) Nijhuis, C. A.; Reus, W. F.; Whitesides, G. M. Molecular Rectification in Metal–SAM–Metal Oxide–Metal Junctions. *J. Am. Chem. Soc.* **2009**, *131*, 17814–17827.
- (29) Reus, W. F.; Thuo, M. M.; Shapiro, N. D.; Nijhuis, C. A.; Whitesides, G. M. The SAM, Not the Electrodes, Dominates Charge Transport in Metal–Monolayer//Ga₂O₃/Gallium–Indium Eutectic Junctions. *ACS Nano* **2012**, *6*, 4806–4822.
- (30) Nerngchamngong, N.; Yuan, L.; Qi, D.-C.; Li, J.; Thompson, D.; Nijhuis, C. A. The Role of van der Waals Forces in the Performance of Molecular Diodes. *Nat. Nanotechnol.* **2013**, *8*, 113–118.
- (31) Thuo, M. M.; Reus, W. F.; Nijhuis, C. A.; Barber, J. R.; Kim, C.; Schulz, M. D.; Whitesides, G. M. Odd–Even Effects in Charge Transport across Self-Assembled Monolayers. *J. Am. Chem. Soc.* **2011**, *133*, 2962–2975.
- (32) Masillamani, A. M.; Crivillers, N.; Orgiu, E.; Rotzler, J.; Bossert, D.; Thippeswamy, R.; Zharnikov, M.; Mayor, M.; Samori, P. Multiscale Charge Injection and Transport Properties in Self-Assembled Monolayers of Biphenyl Thiols with Varying Torsion Angles. *Chem.—Eur. J.* **2012**, *18*, 10335–10347.
- (33) Fracasso, D.; Valkenier, H.; Hummelen, J. C.; Solomon, G. C.; Chiechi, R. C. Evidence for Quantum Interference in SAMs of Arylethynylene Thiolates in Tunneling Junctions with Eutectic Ga–In (EGaIn) Top-Contacts. *J. Am. Chem. Soc.* **2011**, *133*, 9556–9563.
- (34) Yoon, H. J.; Shapiro, N. D.; Park, K. M.; Thuo, M. M.; Soh, S.; Whitesides, G. M. The Rate of Charge Tunneling through Self-Assembled Monolayers Is Insensitive to Many Functional Group Substitutions. *Angew. Chem., Int. Ed.* **2012**, *51*, 4658–4661.
- (35) Yoon, H. J.; Bowers, C. M.; Baghbanzadeh, M.; Whitesides, G. M. The Rate of Charge Tunneling Is Insensitive to Polar Terminal Groups in Self-Assembled Monolayers in AgTSS(CH₂)_nM(CH₂)_mT//Ga₂O₃/EGaIn Junctions. *J. Am. Chem. Soc.* **2013**, *136*, 16–19.
- (36) Fracasso, D.; Muglali, M. L.; Rohwerder, M.; Terfort, A.; Chiechi, R. C. The Influence of an Atom in EGaIn/Ga₂O₃ Tunneling Junctions Comprising Self-Assembled Monolayers. *J. Phys. Chem. C* **2013**, *117*, 11367–11376.
- (37) Liao, K.-C.; Yoon, H. J.; Bowers, C. M.; Simeone, F. C.; Whitesides, G. M. Replacing AgTSSCH₂-R with AgTSO₂C-R in EGaIn-Based Tunneling Junctions Does Not Significantly Change Rates of Charge Transport. *Angew. Chem., Int. Ed.* **2014**, *53*, 3889–3893.
- (38) Bowers, C. M.; Liao, K.-C.; Yoon, H. J.; Rappoport, D.; Baghbanzadeh, M.; Simeone, F. C.; Whitesides, G. M. Introducing Ionic and/or Hydrogen Bonds into the SAM//Ga₂O₃ Top-Interface of

AgTS/S(CH₂)_nT//Ga₂O₃/EGaIn Junctions. *Nano Lett.* **2014**, *14*, 3521–3526.

(39) Thuo, M. M.; Reus, W. F.; Simeone, F. C.; Kim, C.; Schulz, M. D.; Yoon, H. J.; Whitesides, G. M. Replacing –CH₂CH₂– with –CONH– Does Not Significantly Change Rates of Charge Transport through AgTS-SAM//Ga₂O₃/EGaIn Junctions. *J. Am. Chem. Soc.* **2012**, *134*, 10876–10884.

(40) Sedghi, G.; Esdaile, L. J.; Anderson, H. L.; Martin, S.; Bethell, D.; Higgins, S. J.; Nichols, R. J. Comparison of the Conductance of Three Types of Porphyrin-Based Molecular Wires: β ,meso, β -Fused Tapes, meso-Butadiyne-Linked and Twisted meso-meso Linked Oligomers. *Adv. Mater.* **2012**, *24*, 653–657.

(41) Liu, Z.; Yasser, A. A.; Lindsey, J. S.; Bocian, D. F. Molecular Memories That Survive Silicon Device Processing and Real-World Operation. *Science* **2003**, *302*, 1543–1545.

(42) Sedghi, G.; García-Suárez, V. M.; Esdaile, L. J.; Anderson, H. L.; Lambert, C. J.; Martín, S.; Bethell, D.; Higgins, S. J.; Elliott, M.; Bennett, N.; Macdonald, J. E.; Nichols, R. J. Long-range electron tunnelling in oligo-porphyrin molecular wires. *Nat. Nanotechnol.* **2011**, *6*, 517–523.

(43) Wang, C.; Batsanov, A. S.; Bryce, M. R.; Martín, S.; Nichols, R. J.; Higgins, S. J.; García-Suárez, V. M.; Lambert, C. J. Oligoynne Single Molecule Wires. *J. Am. Chem. Soc.* **2009**, *131*, 15647–15654.

(44) Kiguchi, M.; Takahashi, T.; Kanehara, M.; Teranishi, T.; Murakoshi, K. Effect of End Group Position on the Formation of a Single Porphyrin Molecular Junction. *J. Phys. Chem. C* **2009**, *113*, 9014–9017.

(45) Scudiero, L.; Barlow, D. E.; Mazur, U.; Hipps, K. W. Scanning Tunneling Microscopy, Orbital-Mediated Tunneling Spectroscopy, and Ultraviolet Photoelectron Spectroscopy of Metal(II) Tetraphenylporphyrins Deposited from Vapor. *J. Am. Chem. Soc.* **2001**, *123*, 4073–4080.

(46) Duong, B.; Arechabaleta, R.; Tao, N. J. In situ AFM/STM characterization of porphyrin electrode films for electrochemical detection of neurotransmitters. *J. Electroanal. Chem.* **1998**, *447*, 63–69.

(47) Shimazu, K.; Takechi, M.; Fujii, H.; Suzuki, M.; Saiki, H.; Yoshimura, T.; Uosaki, K. Formation and characterization of thiol-derivatized zinc (II) porphyrin monolayers on gold. *Thin Solid Films* **1996**, *273*, 250–253.

(48) Samorí, P.; Diebel, J.; Löwe, H.; Rabe, J. P. Template-Stripped Gold Supported on Ni as a Substrate for SAMs. *Langmuir* **1999**, *15*, 2592–2594.

(49) Mosley, D. W.; Chow, B. Y.; Jacobson, J. M. Solid-State Bonding Technique for Template-Stripped Ultraflat Gold Substrates. *Langmuir* **2006**, *22*, 2437–2440.

(50) Hugall, J. T.; Finnemore, A. S.; Baumberg, J. J.; Steiner, U.; Mahajan, S. Solvent-Resistant Ultraflat Gold Using Liquid Glass. *Langmuir* **2011**, *28*, 1347–1350.

(51) Li, Y. *Microelectronic Applications of Chemical Mechanical Planarization*; John Wiley & Sons: Hoboken, NJ, 2007.

(52) Saif Islam, M.; Jung, G. Y.; Ha, T.; Stewart, D. R.; Chen, Y.; Wang, S. Y.; Williams, R. S. Ultra-Smooth Platinum Surfaces for Nanoscale Devices Fabricated Using Chemical Mechanical Polishing. *Appl. Phys. A: Mater. Sci. Process.* **2005**, *80*, 1385–1389.

(53) Steigerwald, J. M.; Murarka, S. P.; Gutmann, R. J. *Chemical Mechanical Planarization of Microelectronic Materials*; Wiley-VCH: Weinheim, Germany, 2004.

(54) Walker, P.; Tarn, W. H. *CRC Handbook of Metal Etchants*; CRC Press: Boca Raton, FL, 2010.

(55) Strenge, K.; Pilgrim, H. The Desaggregation of Solid Particle Aggregates by Ultrasonication. *Colloid Polym. Sci.* **1983**, *261*, 855–857.

(56) Cumpson, P. J. The Thickogram: A Method for Easy Film Thickness Measurement in XPS. *Surf. Interface Anal.* **2000**, *29*, 403–406.

(57) Ahrlund, S.; Noren, B.; Oskarsson, A. Crystal Structure of Iodo(tetrahydrothiophene)gold(I) at 200 K: A Compound with an Infinite Array of Gold-Gold bonds. *Inorg. Chem.* **1985**, *24*, 1330–1333.

(58) Bravo, B. G.; Michelhaugh, S. L.; Soriaga, M. P.; Villegas, L.; Suggs, D. W.; Stickney, J. L. Anodic Underpotential Deposition and

Cathodic Stripping of Iodine at Polycrystalline and Single-Crystal Gold: Studies by LEED, AES, XPS, and Electrochemistry. *J. Phys. Chem.* **1991**, *95*, 5245–5249.

(59) Porter, M. D.; Bright, T. B.; Allara, D. L.; Chidsey, C. E. D. Spontaneously Organized Molecular Assemblies. 4. Structural Characterization of n-Alkyl Thiol Monolayers on Gold by Optical Ellipsometry, Infrared Spectroscopy, and Electrochemistry. *J. Am. Chem. Soc.* **1987**, *109*, 3559–3568.

(60) Baghbanzadeh, M.; Simeone, F. C.; Bowers, C. M.; Liao, K.-C.; Thuo, M. M.; Baghbanzadeh, M.; Miller, M.; Carmichael, T. B.; Whitesides, G. M. Odd-Even Effects in Charge Transport Across n-Alkanethiolate-Based SAMs. *J. Am. Chem. Soc.*, in press, **2014**, doi: 10.1021/ja509436k.